ICONTECH INTERNATIONAL JOURNAL OF SURVEYS, ENGINEERING, TECHNOLOGY
ISSN 2717-7270
Journal homepage: http://icontechjournal.com/index.php/iij
Volume 6 (2022) Issue 3

Quantum Chemical Characterization of 4-({4-[Bis(2-Cyanoethyl)Amino]Phenyl}Diazinyl)Benzene Sulfonamide by Ab-Initio Calculation

Arini Qurrata Ayun[1*], Pinar Tunay Tasli[1], Hasan Huseyin Kart[2], Sevgi Ozdemir Kart[1*]

[1]Pamukkale University, Science Faculty, Department of Physics, Denizli, Türkiye

[2]Aydın Adnan Menderes University, Science Faculty, Department of Physics, Aydın, Türkiye

[*]*Corresponding author: ariniqurrataayun0@gmail.com and ozsev@pau.edu.tr*

Abstract

4-({4-[Bis(2-cyanoethyl)amino]phenyl}diazinyl)benzene sulfonamide is the azo dye material which has general application in the textile industry. Experimentally, it has been synthesized and geometrically characterized by G. Gervasio et *al*. In this study, the theoretical analysis has been calculated by using the ab-initio method based on the Density Functional Theory/B3LYP/6-311G(d,p) to characterize the structural, spectroscopy, and electronic properties of the title azo dye. Its molecular geometries are in the good agreement with those of available experiment data. 129 vibrational modes have been specified with stretching, in-plane-bending, out-of-plane-bending, and torsion vibration modes by the Potential Energy Distribution analysis. The ultraviolet spectra appear in single peak for six common solvation at ∼429 nm. The Gauge-Invariant Atomic Orbital approach has been applied to predict the chemical shifts of ^{1}H and ^{13}C NMR only in DMSO solvation. The electronic properties have been investigated such as the energy bandgap (3.34 eV), ionization potential energy (6.24 eV), electron affinity (2.90 eV), electronegativity (4.57 eV), and chemical hardness (1.67 eV) by using the Frontier Molecular Orbital Theory from the energy interaction of the Lowest Unoccupied Molecular Orbital and Highest Occupied Molecular Orbital. The characterization of the title azo dye is conducted theoretically for the first time in this study.

Keywords: Density functional theory, UV-Vis absorption, chemical shifts, electronic properties, azo dye.

1. Introduction

4-({4-[Bis(2-cyanoethyl)amino]phenyl}diazinyl)benzene sulfonamide or $C_{18}H_{18}N_6O_2S$ is one of the azo dye family that consists of Nitrogen double bonds [1]. Generally, there is not a standard definition of the term developing azo dye because it can be synthesized from any fiber. However, more than 100.000 different types of azo dye are currently used in recent technology and industrial applications [2] such as in biomedical applications [3], catalyst [4], laser technology [5], industrial dyes [6], degradation material [7], etc.

Experimentally, the title azo dye has been synthesized by G. Gervasio, et al (2010). They have obtained its crystal structure by X-Ray measurement and reported the geometrical parameters of bond length, bond angle, and dihedral angle [8]. However, some spectroscopic and electronic properties have not been measured yet. Therefore, in this study, we have aimed to characterize the title azo dye, 4-({4-[Bis(2-cyanoethyl)amino]phenyl}diazinyl)benzene sulfonamide, by utilizing the quantum chemical computational methods to understand their chemical and physical properties at the atomistic level.

Received 19 August 2022; Received in revised form 6 September 2022; Accepted 14 September 2022;
Available online 25 September 2022;
doi: 10.46291/ICONTECHvol6iss3pp12-29

The computational quantum chemistry is a powerful theoretical method to combine the power of computational technique and the foundation of physics principles to solve and understand chemical problems. This method can simplify and solve many-body electron problems by adding quantum interactions and using some quantum approximations [9]. The effectiveness of the method for azo dye molecules has been confirmed in many studies. Ab-initio calculations have been performed to investigate the potential near-infrared absorbing structures of 2-imidazolyl-2-thiazolyl azo compounds [10]. Funar-Timofei et al. (2012) have aimed to simulate modeling heterocyclic azo dye affinities for cellulose fiber in their study [11]. Atay et al. (2019) have clarified the structural and spectroscopic properties of mono azo dye by performing ab-initio simulations based on density functional theory (DFT) [12]. More recently, some structural and vibrational properties of the azo dye materials have been identified by the ab-initio method based on DFT/B3LYP [13].

In our study, we have performed the ab-initio simulations based on DFT/B3LYP to reveal some spectroscopic and electronic properties of the title azo dye whose structural parameters have been obtained experimentally. The structural parameters have been acquired in terms of bond length, bond angle, and dihedral angle. To validate our results of structural parameters, we have compared them with those of the experiment by using linear regression analysis [14]. The vibrational frequencies and their fundamental modes have been evaluated by calculating FT-IR spectra [15]. UV-Vis absorption spectra of the title azo dye in the excited state have been studied for six common solvation such as water, methanol, ethanol, chloroform, dichloromethane, and dimethyl sulfoxide (DMSO) to see the effect of solvation on the absorption peaks by utilizing time-dependent TD-DFT/B3LYP/6-311G (d,p) method [16]. The chemical shifts of ^{1}H and ^{13}C NMR of the title azo dye have been predicted by using GIAO-DFT/B3LYP/6-311G(d,p) method [17]. Electronic properties such as energy bandgap (Eg), ionization potential energy (IP), electron affinity (EA), electronegativity (x), and chemical hardness (η) have been obtained from HOMO-LUMO relations by using the Frontier Molecular Orbital Theory (FMO) [18]. To the best of our knowledge, the results obtained from the DFT computations are done for the first time, in this study.

2. Computational Method

This research is based on quantum chemical calculations based on the ab initio method, which is a computational method without needing any empirical information about the molecular system [9]. The global energy minima of the title molecule has been obtained by optimizing the molecular structure at the level of the ab-initio method based on DFT within B3LYP exchange-correlation functional (which represents Becke 3-parameter, Lee-Yang-Parr) [19, 20] implemented in the Gaussian 09 Package Program [21, 22]. The electronic-wave function used in DFT is described by 6-311G(d,p) basis set in this study. Figure 1 **(b)** shows the optimized molecular structure of the azo dye molecule with the atomic numbering as well as the schematic view of the synthesized molecule structure. FT-IR (Fourier Transform Infrared Radiation) spectral analysis has been carried out to identify the fundamental vibrational modes of the optimized molecule by utilizing the same method and the basis set. Potential Energy Distribution (PED) for each of the vibrational frequencies has been computed via VEDA4 (Vibrational Energy Distribution Analysis) program designated the character of each mode numerically [23, 24]. It has become customary to multiply the vibrational frequencies by the scaling factor of 0.966 for 6-311G(d,p) basis set because the DFT method overestimates the vibration modes [25]. Time-dependent density functional theory (TD-DFT)/B3LYP based

Received 19 August 2022; Received in revised form 6 September 2022; Accepted 14 September 2022;
Available online 25 September 2022;
doi: 10.46291/ICONTECHvol6iss3pp12-29

simulations have been fulfilled to provide UV-Vis spectrum in the excited state in six different solvation of water, methanol, ethanol, chloroform, dichloromethane, and dimethyl sulfoxide (DMSO) to understand the impact of solvation on the value of the absorption peaks of the title molecule [26, 27]. The chemical shift of the title azo dye has been predicted by investigating the hydrogen and carbon nuclear magnetic resonance (NMR). The Gauge Invariant Atomic Orbitals (GIAO) method has been employed in the medium of DMSO to attain the ^{1}H and ^{13}C NMR shielding constant [28]. Finally, we have investigated the Frontier Molecular Orbital Theory (FMO) analysis to get HOMO-LUMO interactions leading to identifying chemical hardness, chemical softness, ionization potential, electron affinity, electronegativity, electrophilicity, and chemical potential of the title molecule [29].

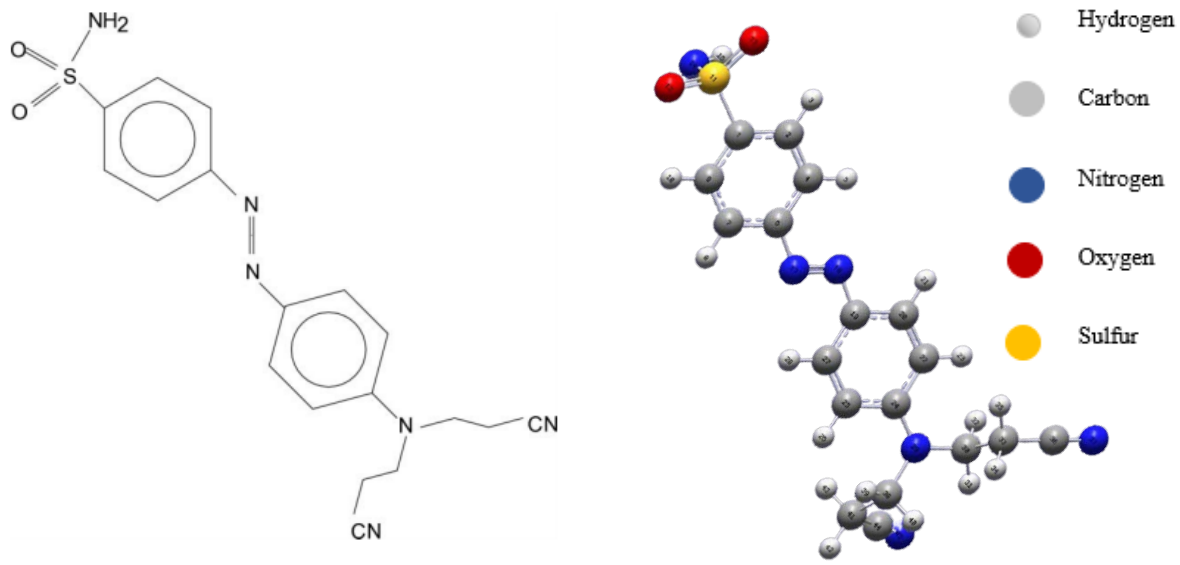

(a) **(b)**

Figure 1. (a) Schematic view of synthesized molecule [8] and **(b)** the optimized structure of the title azo dye via GaussView 5.0 program.

3. Result and Discussion

3.1. Optimized structure

The structure of the title azo dye has been simulated to be achieved its stable structure. Thus, the optimized structure in the ground state has been visualized in three dimensions by using Gauss View 5.0 program. The calculations conducted by using DFT/B3LYP with 6-311G(d,p) basis set are used to predict the structural parameters and vibrational frequencies [30]. The optimized structure of the title azo dye, shown in Figure 1, has 45 atoms (18 carbons, 2 oxygens, 6 nitrogens, 1 sulfur, and 18 hydrogens) and owns 129 fundamental vibrational modes. The structural parameters such as bond length, bond angle, and dihedral angle of the title azo dye are given in Table 1, along with those of the available experiment. As seen in the table, it has 46 bond lengths, 74 bond angles, and 99 dihedral angles, respectively.

Received 19 August 2022; Received in revised form 6 September 2022; Accepted 14 September 2022;
Available online 25 September 2022;
doi: 10.46291/ICONTECHvol6iss3pp12-29

A linear regression analysis has been ensured to examine the correlation between the experiment and the DFT simulation. Linear regression is provided by the linear equation of $y = ax + b$, where a and b are the fit parameters [14, 31]. The result is depicted in Figure 2. The regression values of bond length and bond angle are calculated as 0.968 and 0.926, correspondingly, which indicates that our DFT results of structural parameters are in excellent agreement with those of the experiment.

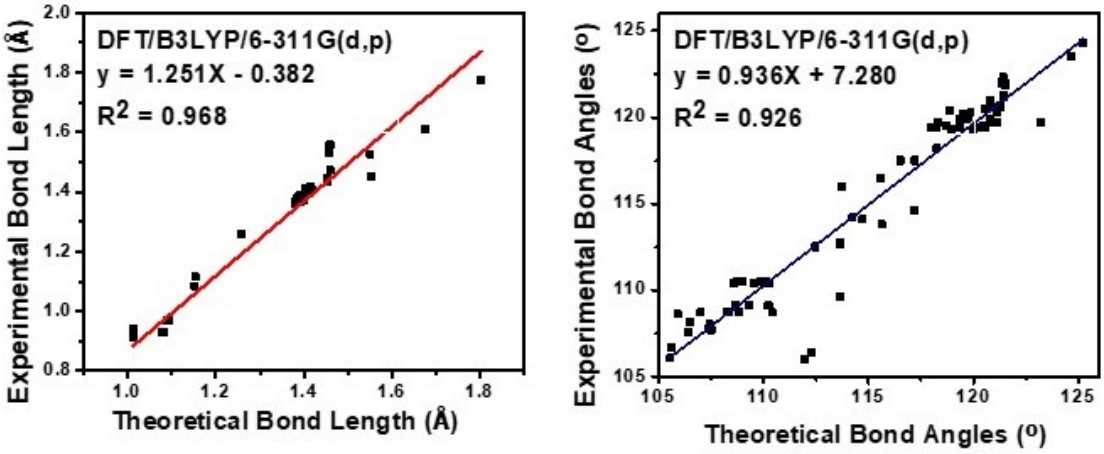

Figure 2. The correlation graphs between observed and calculated of the title molecule parameters both for **(a)** bond length and **(b)** bond angle

Received 19 August 2022; Received in revised form 6 September 2022; Accepted 14 September 2022;
Available online 25 September 2022;
doi: 10.46291/ICONTECHvol6iss3pp12-29

Table 1. The optimized geometrical parameter of the title molecule in the ground state employing DFT/B3LYP/6-311G(d,p) and experimental data. Bond length in (Å), the bond angle and the dihedral angle in (°) [1].

No	Bond length via Gaussian	Symbolic bond labels	DFT/ B3LYP/ 6-311G (d,p)	Exp. data
1	R(1,2)	C1-C2	1.398	1.381
2	R(1,9)	C1-C9	1.393	1.364
3	R(1,11)	C1-S11	1.802	1.775
4	R(2,3)	C2-H3	1.083	0.930
5	R(2,4)	C2-C4	1.386	1.381
6	R(4,5)	C4-H5	1.081	0.930
7	R(4,6)	C4-C6	1.404	1.387
8	R(6,7)	C6-C7	1.399	1.373
9	R(6,17)	C6-N17	1.416	1.419
10	R(7,8)	C7-H8	1.083	0.930
11	R(7,9)	C7-C9	1.390	1.388
12	R(9,10)	C9-H10	1.083	0.930
13	R(11,12)	S11-O12	1.455	1.433
14	R(11,13)	S11-O13	1.455	1.440
15	R(11,14)	S11-N14	1.676	1.610
16	R(14,15)	N14-H15	1.013	0.939
17	R(14,16)	N14-H16	1.012	0.913
18	R(17,18)	N17-N18	1.258	1.259
19	R(18,19)	N18-C19	1.403	1.414
20	R(19,20)	C19-C20	1.399	1.390
21	R(19,27)	C19-C27	1.404	1.393
22	R(20,21)	C20-H21	1.083	0.930
23	R(20,22)	C20-C22	1.384	1.372
24	R(22,23)	C22-H23	1.080	0.930
25	R(22,24)	C22-C24	1.413	1.405
26	R(24,25)	C24-C25	1.419	1.403
27	R(24,29)	C24-N29	1.389	0.930
28	R(25,26)	C25-H26	1.081	0.930
29	R(25,27)	C25-C27	1.380	1.363
30	R(27,28)	C27-H28	1.082	0.930
31	R(29,30)	N29-C30	1.457	1.530
32	R(29,38)	N29-C38	1.455	1.447
33	R(30,31)	C30-H31	1.090	0.970
34	R(30,32)	C30-H32	1.090	0.970
35	R(30,33)	C30-C33	1.551	1.452
36	R(33,34)	C33-H34	1.094	0.970
37	R(33,35)	C33-H35	1.093	0.970
38	R(33,36)	C33-C36	1.459	1.556
39	R(36,37)	C36-H37	1.152	1.085
40	R(38,39)	C38-H39	1.092	0.970
41	R(38,40)	C38-H40	1.091	0.970
42	R(38,41)	C38-C41	1.550	1.527
43	R(41,42)	C41-H42	1.095	0.970
44	R(41,43)	C41-H43	1.093	0.970
45	R(41,44)	C41-C44	1.460	1.472
46	R(44,45)	C44-N45	1.153	1.116

No	Bond angles via Gaussian	Symbolic bond labels	DFT/ B3LYP/ 6-311G (d,p)	Exp. data
1	A(2,1,9)	C2-C1-C9	121.3	120.7
2	A(2,1,11)	C2-C1-S11	119.4	119.4
3	A(9,1,11)	C9-C1-S11	119.3	119.9
4	A(1,2,3)	C1-C2-H3	119.7	119.9
5	A(1,2,4)	C1-C2-C4	119.5	120.2
6	A(3,2,4)	H3-C2-C4	120.8	119.9
7	A(2,4,5)	C2-C4-H5	121.1	120.4
8	A(2,4,6)	C2-C4-C6	119.9	119.3
9	A(5,4,6)	H5-C4-C6	118.9	120.4
10	A(4,6,7)	C4-C6-C7	119.8	120.0
11	A(4,6,17)	C4-C6-N17	124.6	123.5
12	A(7,6,17)	C7-C6-N17	115.6	116.5
13	A(6,7,8)	C6-C7-H8	118.3	119.7
14	A(6,7,9)	C6-C7-C9	120.5	120.5
15	A(8,7,9)	H8-C7-C9	121.1	119.7
16	A(1,9,7)	C1-C9-C7	118.9	119.3
17	A(1,9,10)	C1-C9-H10	119.9	120.3
18	A(7,9,10)	C7-C9-H10	121.1	120.3
19	A(1,11,12)	C1-S11-O12	107.4	108.0
20	A(1,11,13)	C1-S11-O13	107.5	107.7
21	A(1,11,14)	C1-S11-N14	106.5	108.1
22	A(12,11,13)	O12-S11-O13	123.2	119.7
23	A(12,11,14)	O12-S11-N14	105.6	106.7
24	A(13,11,14)	O13-S11-N14	105.7	106.1
25	A(11,14,15)	S11-N14-H15	113.6	109.6
26	A(11,14,16)	S11-N14-H16	113.6	112.7
27	A(15,14,16)	H15-N14-H16	113.7	116.0
28	A(6,17,18)	C6-N17-N18	114.7	114.1
29	A(17,18,19)	N17-N18-C19	115.6	113.8
30	A(18,19,20)	N18-C19-C20	116.5	117.5
31	A(18,19,27)	N18-C19-C27	125.2	124.3

Received 19 August 2022; Received in revised form 6 September 2022; Accepted 14 September 2022;
Available online 25 September 2022;
doi: 10.46291/ICONTECHvol6iss3pp12-29

Table 1. (Continued)

32	A(20,19,27)	C20-C19-C27	118.2	118.2
33	A(19,20,21)	C19-C20-H21	118.2	119.4
34	A(19,20,22)	C19-C20-C22	121.4	121.2
35	A(21,20,22)	H21-C20-C22	120.3	119.4
36	A(20,22,23)	C20-C22-H23	118.3	119.7
37	A(20,22,24)	C20-C22-C24	120.9	120.6
38	A(23,22,24)	H23-C22-C24	120.9	119.7
39	A(22,24,25)	C22-C24-C25	117.2	117.5
40	A(22,24,29)	C22-C24-N29	121.5	121.9
41	A(25,24,29)	C25-C24-N29	121.3	120.6
42	A(24,25,26)	C24-C25-H26	120.6	119.4
43	A(24,25,27)	C24-C25-C27	121.4	121.3
44	A(26,25,27)	H26-C25-C27	117.9	119.4
45	A(19,27,25)	C19-C27-C25	120.8	121.0
46	A(19,27,28)	C19-C27-H28	118.7	119.5
47	A(25,27,28)	C25-C27-H28	120.5	119.5
48	A(24,29,30)	C24-N29-C30	121.4	122.3
49	A(24,29,38)	C24-N29-C38	121.4	122.0
50	A(30,29,38)	C30-N29-C38	117.2	114.6
51	A(29,30,31)	N29-C30-H31	108.6	110.4
52	A(29,30,32)	N29-C30-H32	110.3	110.4
53	A(29,30,33)	N29-C30-C33	112.3	106.4
54	A(31,30,32)	H31-C30-H32	105.9	108.6
55	A(31,30,33)	H31-C30-C33	109.5	110.4
56	A(32,30,33)	H32-C30-C33	110.0	110.4
57	A(30,33,34)	C30-C33-H34	109.9	110.5
58	A(30,33,35)	C30-C33-H35	110.1	110.5
59	A(30,33,36)	C30-C33-C36	111.9	106.00
60	A(34,33,35)	H34-C33-H35	107.0	108.70
61	A(34,33,36)	H34-C33-C36	108.8	110.50
62	A(35,33,36)	H35-C33-C36	108.9	110.50
63	A(29,38,39)	N29-C38-H39	110.4	108.70
64	A(29,38,40)	N29-C38-H40	108.2	108.70
65	A(29,38,41)	N29-C38-C41	114.2	114.20
66	A(39,38,40)	H39-C38-H40	106.4	107.60
67	A(39,38,41)	H39-C38-C41	108.3	108.70
68	A(40,38,41)	H40-C38-C41	108.9	108.70
69	A(38,41,42)	C38-C41-H42	109.3	109.10
70	A(38,41,43)	C38-C41-H43	110.2	109.10
71	A(38,41,44)	C38-C41-C44	112.5	112.50
72	A(42,41,43)	H42-C41-H43	107.4	107.80

Table 1. (Continued)

73	A(42,41,44)	H42-C41-C44	108.7	109.10
74	A(43,41,44)	H43-C41-C44	108.6	109.10

No	Dihedral angles via Gaussian	Symbolic bond labels	DFT/ B3LYP/ 6-311G (d,p)
1	D(9,1,2,3)	C9-C1-C2-H3	-177.47
2	D(9,1,2,4)	C9-C1-C2-C4	0.78
3	D(11,1,2,3)	S11-C1-C2-H3	3.14
4	D(11,1,2,4)	S11-C1-C2-C4	-178.61
5	D(2,1,9,7)	C2-C1-C9-C7	-0.68
6	D(2,1,9,10)	C2-C1-C9-H10	177.65
7	D(11,1,9,7)	S11-C1-C9-C7	178.70
8	D(11,1,9,10)	S11-C1-C9-H10	-2.96
9	D(2,1,11,12)	C2-C1-S11-O12	-158.84
10	D(2,1,11,13)	C2-C1-S11-O13	-24.37
11	D(2,1,11,14)	C2-C1-S11-N14	88.39
12	D(9,1,11,12)	C9-C1-S11-O12	21.76
13	D(9,1,11,13)	C9-C1-S11-O13	156.23
14	D(9,1,11,14)	C9-C1-S11-N14	-91.00
15	D(1,2,4,5)	C1-C2-C4-H5	-179.55
16	D(1,2,4,6)	C1-C2-C4-C6	-0.09
17	D(3,2,4,5)	H3-C2-C4-H5	-1.32
18	D(3,2,4,6)	H3-C2-C4-C6	178.14
19	D(2,4,6,7)	C2-C4-C6-C7	-0.67
20	D(2,4,6,17)	C2-C4-C6-N17	-179.85
21	D(5,4,6,7)	H5-C4-C6-C7	178.79
22	D(5,4,6,17)	H5-C4-C6-N17	-0.38
23	D(4,6,7,8)	C4-C6-C7-H8	-178.81
24	D(4,6,7,9)	C4-C6-C7-C9	0.77
25	D(17,6,7,8)	N17-C6-C7-H8	0.44
26	D(17,6,7,9)	N17-C6-C7-C9	-179.98
27	D(4,6,17,18)	C4-C6-N17-N18	-2.75
28	D(7,6,17,18)	C7-C6-N17-N18	178.04
29	D(6,7,9,1)	C6-C7-C9-C1	-0.10
30	D(6,7,9,10)	C6-C7-C9-H10	-178.41
31	D(8,7,9,1)	H8-C7-C9-C1	179.47
32	D(8,7,9,10)	H8-C7-C9-H10	1.15
33	D(1,11,14,15)	C1-S11-N14-H15	65.77
34	D(1,11,14,16)	C1-S11-N14-H16	-66.35
35	D(12,11,14,15)	O12-S11-N14-H15	-48.24
36	D(12,11,14,16)	O12-S11-N14-H16	179.62
37	D(13,11,14,15)	O13-S11-N14-H15	179.87
38	D(13,11,14,16)	O13-S11-N14-H16	47.74
39	D(6,17,18,19)	C6-N17-N18-C19	179.78

Received 19 August 2022; Received in revised form 6 September 2022; Accepted 14 September 2022;
Available online 25 September 2022;
doi: 10.46291/ICONTECHvol6iss3pp12-29

Table 1. (Continued)

40	D(17,18,19,20)	N17-N18-C19-C20	178.60
41	D(17,18,19,27)	N17-N18-C19-C27	-1.45
42	D(18,19,20,21)	N18-C19-C20-H21	0.20
43	D(18,19,20,22)	N18-C19-C20-C22	-179.89
44	D(27,19,20,21)	C27-C19-C20-H21	-179.75
45	D(27,19,20,22)	C27-C19-C20-C22	0.16
46	D(18,19,27,25)	N18-C19-C27-C25	179.78
47	D(18,19,27,28)	N18-C19-C27-H28	-0.06
48	D(20,19,27,25)	C20-C19-C27-C25	-0.28
49	D(20,19,27,28)	C20-C19-C27-H28	179.89
50	D(19,20,22,23)	C19-C20-C22-H23	-179.87
51	D(19,20,22,24)	C19-C20-C22-C24	0.15
52	D(21,20,22,23)	H21-C20-C22-H23	0.03
53	D(21,20,22,24)	H21-C20-C22-C24	-179.94
54	D(20,22,24,25)	C20-C22-C24-C25	-0.33
55	D(20,22,24,29)	C20-C22-C24-N29	179.64
56	D(23,22,24,25)	H23-C22-C24-C25	179.69
57	D(23,22,24,29)	H23-C22-C24-N29	-0.34
58	D(22,24,25,26)	C22-C24-C25-H26	-179.88
59	D(22,24,25,27)	C22-C24-C25-C27	0.22
60	D(29,24,25,26)	N29-C24-C25-H26	0.15
61	D(29,24,25,27)	N29-C24-C25-C27	-179.75
62	D(22,24,29,30)	C22-C24-N29-C30	0.20
63	D(22,24,29,38)	C22-C24-N29-C38	177.65
64	D(25,24,29,30)	C25-C24-N29-C30	-179.83
65	D(25,24,29,38)	C25-C24-N29-C38	-2.38
66	D(24,25,27,19)	C24-C25-C27-C19	0.08
67	D(24,25,27,28)	C24-C25-C27-H28	179.92
68	D(26,25,27,19)	H26-C25-C27-C19	-179.82
69	D(26,25,27,28)	H26-C25-C27-H28	0.01
70	D(24,29,30,31)	C24-N29-C30-H31	-155.79
71	D(24,29,30,32)	C24-N29-C30-H32	-40.19
72	D(24,29,30,33)	C24-N29-C30-C33	82.94
73	D(38,29,30,31)	C38-N29-C30-H31	26.65
74	D(38,29,30,32)	C38-N29-C30-H32	142.26
75	D(38,29,30,33)	C38-N29-C30-C33	-94.61
76	D(24,29,38,39)	C24-N29-C38-H39	-40.02
77	D(24,29,38,40)	C24-N29-C38-H40	-156.16
78	D(24,29,38,41)	C24-N29-C38-C41	82.37
79	D(30,29,38,39)	C30-N29-C38-H39	137.53
80	D(30,29,38,40)	C30-N29-C38-H40	21.39
81	D(30,29,38,41)	C30-N29-C38-C41	-100.07
82	D(29,30,33,34)	N29-C30-C33-H34	60.35
83	D(29,30,33,35)	N29-C30-C33-H35	-57.29
84	D(29,30,33,36)	N29-C30-C33-C36	-178.66

Table 1. (Continued)

85	D(31,30,33,34)	H31-C30-C33-H34	-60.36
86	D(31,30,33,35)	H31-C30-C33-H35	-178.00
87	D(31,30,33,36)	H31-H30-C33-C36	60.63
88	D(32,30,33,34)	H32-C30-C33-H34	-176.39
89	D(32,30,33,35)	H32-C30-C33-H35	65.97
90	D(32,30,33,36)	H32-C30-C33-C36	-55.41
91	D(29,38,41,42)	N29-C38-C41-H42	-175.21
92	D(29,38,41,43)	N29-C38-C41-H43	-57.41
93	D(29,38,41,44)	N29-C38-C41-C44	63.98
94	D(39,38,41,42)	H39-C38-C41-H42	-51.69
95	D(39,38,41,43)	H39-C38-C41-H43	66.11
96	D(39,38,41,44)	H39-C38-C41-C44	-172.50
97	D(40,38,41,42)	H40-C38-C41-H42	63.66
98	D(40,38,41,43)	H40-C38-C41-H43	-178.54
99	D(40,38,41,44)	H40-C38-C41-C44	-57.15

Received 19 August 2022; Received in revised form 6 September 2022; Accepted 14 September 2022;
Available online 25 September 2022;
doi: 10.46291/ICONTECHvol6iss3pp12-29

3.2. FT-IR and Vibrational Modes

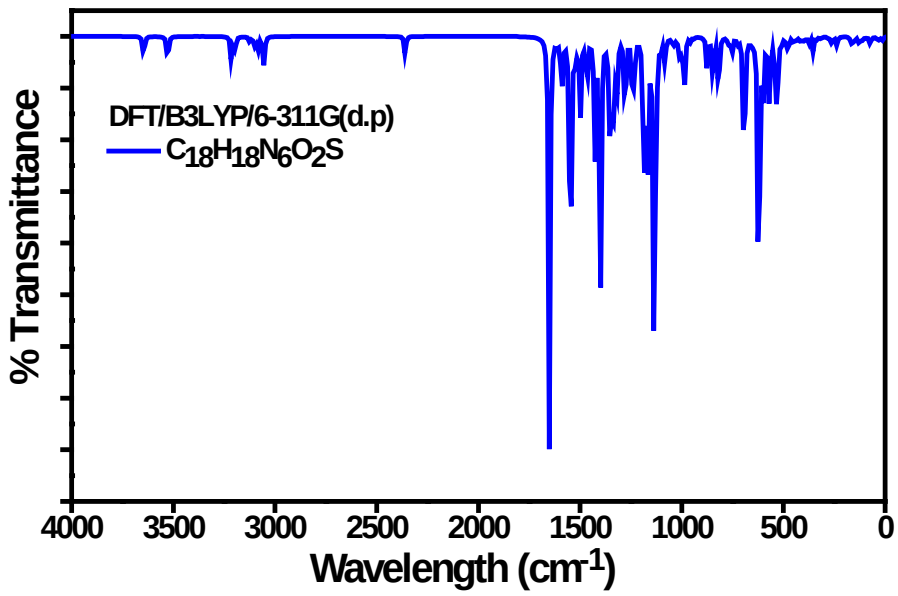

Figure 3. FT-IR Spectra of the title azo dye simulating by DFT/B3LYP/6-311G(d,p).

The determination of the vibrational frequencies employing quantum chemistry methods is becoming an increasingly important tool. Theoretically predicted frequencies can provide ones to determine the fingerprints of the chemical compounds [32]. It also shows important information about the nature of the chemical and molecular bond, intramolecular forces acting between the atoms, and intermolecular forces in the condensed phase. A molecule can vibrate in many ways, and each way is called a vibrational mode [33, 34]. The vibrational modes can be defined as a way of vibrating when applied to a system that has several points with different amplitudes of deflection [35]. The absolute IR intensities of the transmittance for the optimized structure as a function of harmonic vibrational wavenumbers are attained by DFT/B3LYP/6-311G(d,p). The infrared spectrum is given in Figure 3 with 45 atoms and 129 fundamentals vibration modes. The normal mode assignments of the vibrational modes are performed by combining the GAUSSVIEW 5.0 package software and VEDA4 programs [36]. Table 2 collects some specific and important vibrational modes, as well as the assignment of fundamental vibrational modes. The experimental measurements of fingerprint regions for the title azo dye considered in this work are compared with the theoretical data obtained from the quantum chemistry method. Some important vibrational modes can be analyzed such as vibration between nitrogen and hydrogen (ν NH) band in the region of 3525 – 3411 cm^{-1}, vibration aromatic between carbon and hydrogen (ν_{AR} NH) band in the region of 3111 – 3021 cm^{-1}, and vibration between nitrogen double bond (ν NN) band in the region of 1496 - 1448 cm^{-1}. As seen in Table 2, these vibrational modes are found in these regions by using the computational quantum chemistry method used in this work.

Received 19 August 2022; Received in revised form 6 September 2022; Accepted 14 September 2022;
Available online 25 September 2022;
doi: 10.46291/ICONTECHvol6iss3pp12-29

Table 2. Vibrational modes of the title azo dye computed by DFT/B3LYP/6-311G(d,p) in the unit of cm^{-1}. IR intensities ($km.mol^{-1}$) and assignment with PED (obtained from DFT/B3LYP/6-311G(d,p)) percentage in the brackets with scale factors as 0.967.

Mod	Freq		I^{IR}	Assignment [PED]>10%
	Unscaled	Scaled		
1	10.950	10.5900	3.6700	τ NNCC (51) + τ CCNN (25)
2	16.500	15.9600	1.7400	τ CCCC (16) + τ CNNC (21) + γ CCCN (15) + γ CCNC (13) + γ NCCC (10)
3	27.930	27.0100	4.6000	δ NNC (11) + δ CNN (11) + τ CCCN (29)
4	32.280	31.2100	0.3200	τ CNNC (12) + τ CCCN (17) + τ CCNC (24)
5	39.170	37.8800	1.4400	τ CNCC (11) + τ NSCC (17)
6	44.320	42.8600	0.9900	τ CCCN (15) + τ NSCC (54)
7	49.250	47.6200	0.1400	τ NNCC (11) + τ CCCN (20) + τ NSCC (20)
8	63.720	61.6200	2.6000	τ CCNC (18)
9	74.310	71.8600	8.2500	τ CCCN (34) + τ CNCC (30)
10	90.020	87.0500	1.9800	τ CCCN (32)

Table 2. (Continued)

11	108.95	105.350	5.1700	τ CCCN (20) + τ CCNC (37)
12	120.45	116.470	3.7100	δ CCN (10) + δ CCC (14)
13	130.76	126.440	6.1200	δ NSC (17) + τ CCNN (12) + γ SCCC (22)
14	152.65	147.610	8.9600	δ NCC (17) + δ CCC (34)
15	164.23	158.810	8.0100	δ SCC (30) + γ ONCS (12)
16	175.59	169.800	1.5100	δ CCC (10) + τ CCNN (13) + τ CCCC (10)
17	206.14	199.340	0.2700	τ CCCC (10)
18	232.31	224.640	2.7500	δ NCC (12)
19	239.15	231.260	9.6000	δ NSC (28) + τ CCCC (18)
20	261.83	253.190	10.760	δ OSN (14) + τ HNSC (26) + τ HNSC (15)
21	277.89	268.720	3.1800	δ CCN (40)
22	315.31	304.900	3.7100	δ NCC (12) + δ CNC (15)
23	334.54	323.500	4.1800	ν SC (14)
24	354.10	342.410	17.060	
25	374.96	362.590	9.2000	
26	382.91	370.270	0.3800	τ HCCN (51) + τ NCCC (26)
27	388.27	375.460	0.4300	τ HCCN (48) + τ NCCC (24)

Received 19 August 2022; Received in revised form 6 September 2022; Accepted 14 September 2022;
Available online 25 September 2022;
doi: 10.46291/ICONTECHvol6iss3pp12-29

Table 2. (Continued)

28	396.65	383.560	6.5200	δ OSN (16) + δ SCC (12) + γ ONCS (24)
29	413.18	399.540	7.6400	τ CCCC (12)
30	422.19	408.260	2.0900	τ CCCC (61)
31	435.85	421.470	2.9900	δ CNC (14) + τ CCCC (11)
32	448.79	433.980	5.5900	δ OSN (19) + γ ONCS (16)
33	452.12	437.200	3.1600	δ CNC (15)
34	475.51	459.820	11.790	δ NCC (10) + δ OSO (21)
35	483.87	467.900	11.520	δ NCC (25) + δ OSO (10)
36	511.22	494.350	8.3100	δ CNC (12)
37	531.07	513.540	118.50	τ HNSC (29) + γ ONOS (10)
38	533.12	515.530	12.080	δ OSO (10) + γ NCCC (15)
39	544.17	526.210	17.370	δ CCN (14) + δ CNN (12) + δ NCC (11)
40	566.37	547.680	39.370	τ CNNC (10) + γ SCCC (+12) + γ NCCC (21)
41	572.13	553.250	56.220	δ CCC (10)
42	600.17	580.360	75.700	δ NCC (15) + δ CCC (17) + δ CCN (14)
43	621.04	600.550	447.95	γ ONOS (28)
44	641.39	620.220	0.6334	δ CCC (65)
45	655.58	633.950	4.9496	δ CCC (21) + δ CCN (10)
46	692.90	670.030	210.45	ν SC (14) + δ CCC (10)
47	725.96	702.000	6.8367	τ CCCC (55)
48	751.64	726.840	10.817	γ NCCC (14)
49	755.81	730.870	12.133	δ CCC (11) + γ NCCC (12)
50	771.54	746.080	9.1540	τ HCNC (14) + τ HCCN (25) + τ NCCC (35)
51	817.72	790.730	35.506	ν SN (37)
52	818.64	791.620	32.458	ν SN (23) + τ HCCN (19) + τ HCCC (20)

Table 2. (Continued)

53	822.24	795.110	18.050	ν CC (28) + ν CC (20) + τ HCCC (10)
54	845.67	817.760	39.330	τ HCCN (61)
55	848.68	820.670	21.970	ν CC (10) + δ CCC (19)
56	859.70	831.330	1.7300	τ HCCS (52) + τ HCCC (47)
57	875.52	846.630	38.410	τ HCCS (51) + γ NCCC (13)
58	893.47	863.980	0.8000	ν CC (12) + τ HCCN (15) + τ NCCC (22)
59	940.51	909.470	1.5500	ν CC (17) + δ NNC (16) + δ CCC (11) + δ CNN (16)
60	956.61	925.040	5.4200	ν CC (66)
61	982.93	950.490	12.570	τ HCCC (44) + τ HCCN (15) + τ CCCC (17)
62	988.07	955.460	65.790	ν CC (10) + ν NC (16)
63	990.51	957.820	1.1900	τ HCCC (40) + τ HCCS (40)
64	999.08	966.110	13.580	ν CC (71)
65	1004.67	971.520	2.9000	τ HCCC (47) + τ CCCC (15)
66	1009.76	976.440	22.770	ν CC (42) + τ HCCC (+10)
67	1012.53	979.120	0.6400	τ HCCS (34) + τ HCCC (49)
68	1017.00	983.439	1.6000	δ CCC (67)
69	1025.23	991.397	5.1800	δ CCC (77)
70	1042.46	1008.06	12.300	
71	1073.23	1037.81	1.0200	δ HNS (85)
72	1082.19	1046.48	29.290	ν CC (40) + ν SO (31)
73	1102.76	1066.37	9.4400	δ HCC (15) + τ HCCN (21)
74	1122.42	1085.38	25.960	ν CC (32) + δ HCC (46)
75	1134.89	1097.44	515.12	ν SO (60)

Received 19 August 2022; Received in revised form 6 September 2022; Accepted 14 September 2022;
Available online 25 September 2022;
doi: 10.46291/ICONTECHvol6iss3pp12-29

76	1145.84	1108.03	5.4100	δ HCC (38)

Table 2. (Continued)

77	1164.09	1125.68	134.94	ν NC (13) + δ HCC (27)
78	1179.67	1140.74	212.89	δ HCC (33)
79	1190.14	1150.87	67.710	ν NC (30) + δ HCC (11)
80	1222.16	1181.83	0.1800	ν NC (22) + δ HCC (11)
81	1234.06	1193.34	73.270	δ HCC (24) + τ HCCN (21)
82	1245.59	1204.49	41.260	δ HCC (40)
83	1277.83	1235.66	119.102	ν NC (13) + δ HCC (21)
84	1284.44	1242.05	4.4700	ν NC (15) + δ HCC (13)
85	1308.81	1265.62	1.2800	δ HCC (10) + δ HCH (16) + τ HCNC (28) + τ HCCN (16)
86	1315.66	1272.24	12.960	δ HCC (80)
87	1321.46	1277.85	78.720	δ HCC (40) + τ HCNC (25)
88	1334.58	1290.54	67.380	ν CC (30) + ν SO (30)
89	1342.46	1298.16	84.830	δ HCC (38)
90	1352.27	1307.65	40.680	ν CC (10)
91	1355.64	1310.90	69.360	ν CC (13) + ν SO (44)
92	1366.83	1321.72	7.3300	δ HCC (20)
93	1394.75	1348.72	33.010	δ HCC (11) + τ HCNC (44)
94	1401.65	1355.40	374.17	δ HCC (33) + τ HCNC (32)
95	1426.60	1379.52	117.30	δ HCC (11)
96	1429.83	1382.65	24.140	ν CC (22)
97	1463.94	1415.63	43.520	ν CC (31) + δ HCC (10) + δ HCH (11)
98	1469.49	1421.00	15.780	δ HCH (71)
99	1476.56	1427.83	6.6700	δ HCH (77)
100	1497.66	1448.24	81.460	ν NN (20) + δ HCC (15)

Table 2. (Continued)

101	1504.35	1454.71	13.480	δ HCH (54)
102	1521.55	1471.34	28.860	ν NN (29) + δ HCC (12)
103	1528.72	1478.27	7.1100	δ HCH (67)
104	1547.18	1496.12	389.21	ν NN (10) + ν NC (13) + δ HCC (14)
105	1587.16	1534.78	45.850	δ HNH (84)
106	1594.93	1542.30	22.560	ν CC (54)
107	1612.13	1558.93	7.6700	ν CC (51) + δ CCC (10)
108	1633.00	1579.11	0.4400	ν CC (55)
109	1650.46	1595.99	469.62	ν CC (54)
110	2359.17	2281.32	9.1900	ν NC (90) + ν CC (10)
111	2360.68	2282.78	14.060	ν NC (90) + ν CC (10)
112	3045.70	2945.19	2.8700	ν CH (96)
113	3045.70	2945.19	2.8700	ν CH (97)
114	3048.12	2947.53	1.1000	ν CH (92)
115	3056.84	2955.96	37.590	ν CH (93)
116	3085.47	2983.65	0.9500	ν CH (92)
117	3088.54	2986.62	5.8700	ν CH (88)
118	3102.48	3000.10	13.340	ν NC (20) + ν CH (72)
119	3124.31	3021.21	7.6100	ν CH (91)
120	3189.57	3084.31	3.9800	ν CH (89)
121	3191.20	3085.89	1.3400	ν CH (94)
122	3194.49	3089.07	0.0600	ν CH (87)
123	3198.86	3093.30	12.530	ν CH (98)
124	3213.48	3107.44	0.8400	ν CH (99)
125	3213.48	3107.44	8.9300	ν CH (90)
126	3215.46	3109.35	21.990	ν CH (82)
127	3216.80	3110.65	0.5900	ν CH (92)
128	3527.87	3411.45	37.780	ν NH (100)
129	3645.40	3525.10	29.840	ν NH (100)

3.3. UV absorbance

Absorption spectra are the beam reduction measurement after it has been reflected from a sample surface or passed through a sample. When ultraviolet and visible light is sent into the material, the atoms go into excitation states. In this case, it absorbs some part of the light. This method measures the wavelength at which it absorbs light [37, 38]. Therefore, this method can be used to characterize the structure of chemical material [15]. The energetical stability of the azo dye is strongly dependent on the nature of the media or the solvation. Therefore, in this work, the absorption spectra of the title molecule have been studied in different solvation such as water, methanol, ethanol, chloroform, dichloromethane, and DMSO. The results are displaced in Figure 4. As shown in the figure, the absorbance spectra reveal the main peak at a similar wavelength for six different solvation. However, we have seen that the solvation does not have a strong effect on the wavelength at the maximum absorbance ($\lambda_{\max}$). The values of

Received 19 August 2022; Received in revised form 6 September 2022; Accepted 14 September 2022; Available online 25 September 2022;
doi: 10.46291/ICONTECHvol6iss3pp12-29

the maximum absorbance for six solvation are summarized in Table 3. As seen in the figures, the absorption spectrums in all solvation are very close to each other for the compound. When the theoretical UV spectra for the title azo dye are examined, a single peak is observed in all solvation. There is no tautomer change in different solvation and the structure of the compound is not changed. The UV peak at 400-500 nm indicates that the compound is colored and that there is a chromophore group in its molecular structure.

Table 3. The wavelengths at the maximum absorbance (λ_{max}) for different solvation.

No	Solvation	λ_{max} (nm)	No	Solvation	λ_{max} (nm)
1	Water	429.14	**4**	DMSO	431.36
2	Methanol	428.31	**5**	Dichloromethane	428.26
3	Ethanol	428.97	**6**	Chloroform	425.68

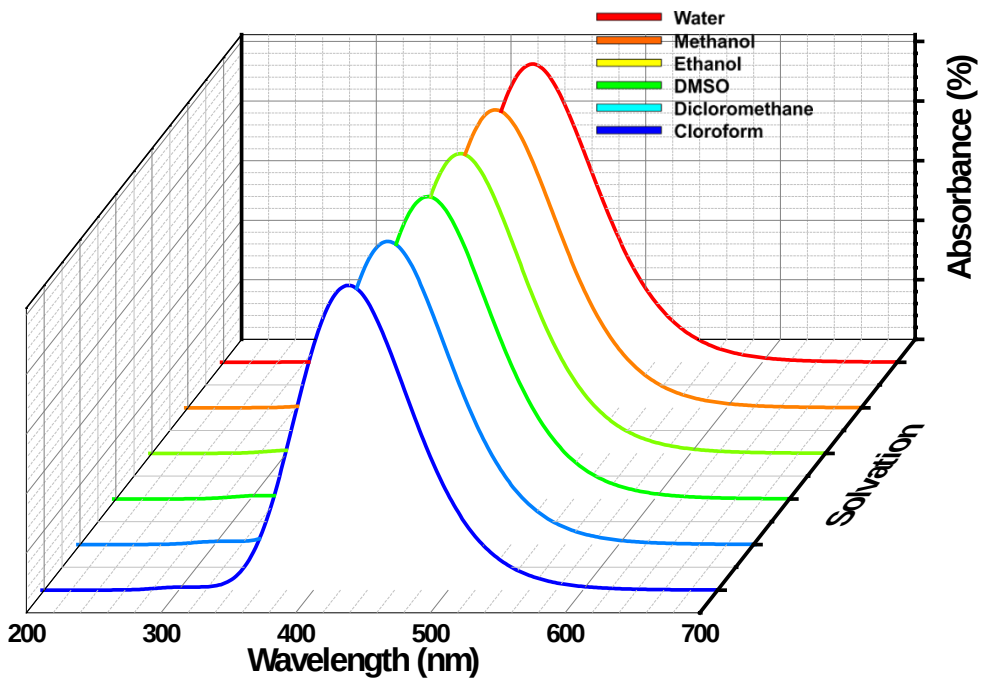

Figure 4. Absorption spectra of the title molecule obtained by TD-DFT/B3LYP/6-311G(d,p) for different solvation.

Carbon and Hydrogen NMR Spectra

Nuclear Magnetic Resonance (NMR) spectroscopy is remarkable tool for providing the valuable information on crystallography or structure of the molecules [39, 40]. Therefore, ^{1}H and ^{13}C NMR chemical shifts can be used as the chemical group characterization of the molecule [41, 42]. The type of spectrum observed depends on the activation energy separating the molecules (which determines the lifetimes of the states) and the chemical shift difference. The computations of ^{1}H and ^{13}C chemical shifts with respect to Tetramethyl-silane (TMS) are performed as implemented GIAO approach at the level of B3LYP and DFT method with 6-311G (d,p) basis set of the title azo dye in the medium of DMSO [43, 44]. The results of the ^{1}H

Received 19 August 2022; Received in revised form 6 September 2022; Accepted 14 September 2022;
Available online 25 September 2022;
doi: 10.46291/ICONTECHvol6iss3pp12-29

and ^{13}C chemical shifts are listed in Table 4. According to the results of the ^{1}H -NMR calculations for our title azo dye; while the peak of CH_2 protons is observed in the region of 3.97 and 2.28 ppm, the peak of the protons in the aromatic rings is between 8.20 – 6.98 ppm and the peak of the proton bound to N is 3.73 ppm.

Table 4. The chemical shifts of ^{1}H and ^{13}C NMR in the medium of DMSO by employing TD-DFT/B3LYP 6-311G(d,p) (all values in ppm).

^{13}C-NMR (ppm)		**^{1}H-NMR (ppm)**	
Atomic Symbol	**DFT/B3LYP/6-311G(d,p)**	**Atomic Symbol**	**DFT/B3LYP/6-311G(d,p)**
C6	158.69	**H8**	8.20
C24	154.81	**H21**	8.20
C1	151.52	**H28**	8.10
C19	148.62	**H5**	8.08
C20	142.11	**H10**	7.99
C7	136.56	**H3**	7.83
C9	130.63	**H23**	6.98
C2	129.98	**H26**	6.68
C44	123.58	**H32**	3.97
C36	121.46	**H31**	3.77
C27	119.23	**H39**	3.76
C4	116.54	**H16**	3.75
C25	114.73	**H15**	3.73
C22	114.02	**H40**	3.47
C30	50.470	**H43**	2.74
C38	48.680	**H35**	2.62
C41	15.860	**H34**	2.39
C33	13.150	**H42**	2.28

Labels of the atoms in this table are given according to figure 1 used in the assignment of the chemical shift

HOMO-LUMO Energy and Electronic Properties

Determining the molecular structure and energies makes it easier to control the chemical reactivity behavior of molecules using the Frontier Molecular Orbital (FMO) Theory [18]. FMO Theory is an efficient method of obtaining the HOMO-LUMO interaction The difference between the HOMO (the highest occupied molecular orbital) and LUMO (the lowest unoccupied molecular orbital) orbital levels defines the energy bandgap, which is an important parameter in assigning the electrical and optical properties of the material [45, 46, 47].

Received 19 August 2022; Received in revised form 6 September 2022; Accepted 14 September 2022; Available online 25 September 2022;
doi: 10.46291/ICONTECHvol6iss3pp12-29

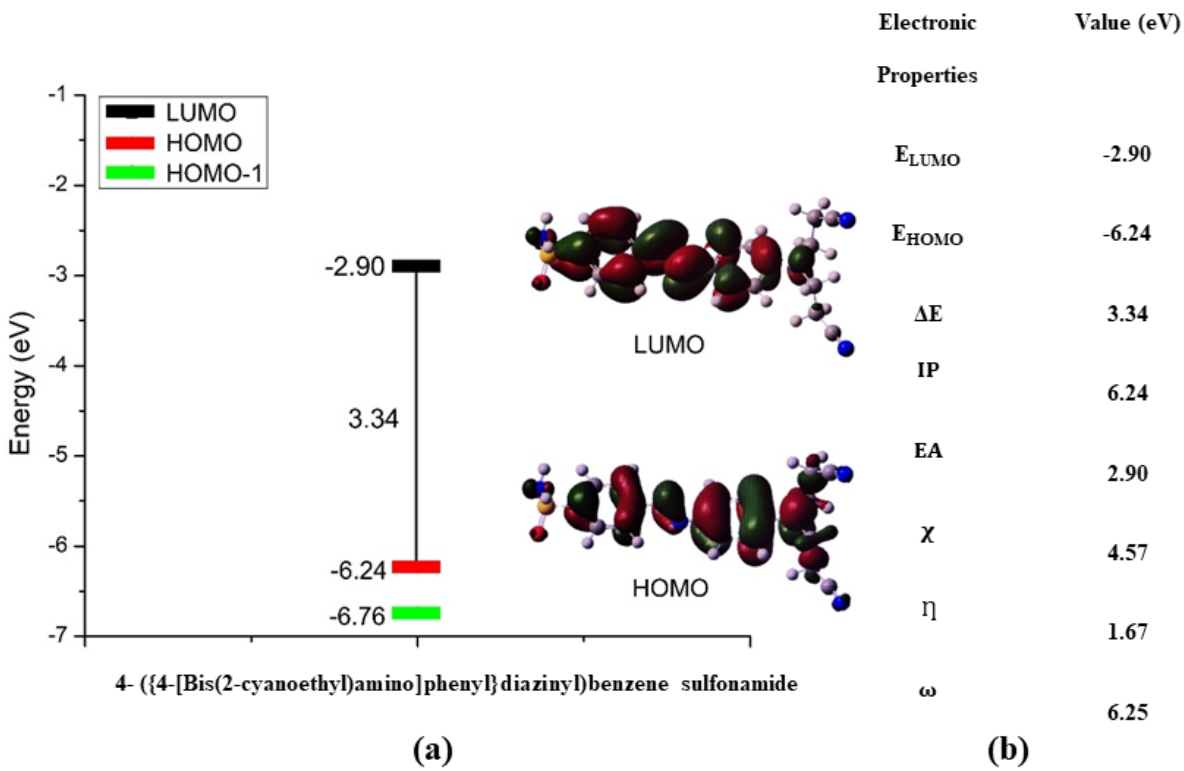

Figure 5. (a) Schematic view of HOMO-LUMO (E_{HOMO} - E_{LUMO}) and energy bandgap (E_g) and (b) the values of some electronic properties: the ionization potential energy (IP), electron affinity (EA), electronegativity (χ), chemical hardness (η) and global electrophilicity index (ω).

The electronic structure parameters of the molecules such as the ionization potential energy (IP) [48], electron affinity (EA) [49], electronegativity (χ) [50], chemical hardness (η) [51], and global electrophilicity index (ω) [52] have been computed from the values of HOMO-LUMO interactions to collect the valuable information about the reactivity of the title compound in this study. The schematic view of HOMO-LUMO levels and energy bandgap, and the values of the electronic properties are presented in Figure 5. The values of HOMO and LUMO levels are evaluated as -6.24 eV and -2.90 which gives rise to calculating the energy bandgap (E_g) as 3.34 eV. This value which is greater than 1.50 eV ensures that the molecule is thermodynamically stable and prevents it from polymerizing.

The ionization potential energy (I = -E_{HOMO}) represents the minimum energy required to take away an electron from the molecule, while the electron affinity (A = -E_{LUMO}) is the energy gained when an electron is added to the system. Electronegativity ($\chi = (I + A)/2$) measures the value of the attraction of an atom for bonding the electrons in the molecules. Chemical hardness ($\eta = (I - A)/2$) shows the degree of the resistance to charge transfer in the molecule. The global electrophilicity index ($\omega = \chi^2/2\eta$) evaluates the tendency of electron acceptors to gain the additional electronic charge. It can be obtained from DFT computations that this molecule has high ionization potential energy of $IP = 6.24\ eV$, a high electron affinity value of $EA =$ 2.90 eV, a strong electronegativity $\chi = 4.57\ eV$, and low chemical hardness η = $1.67\ eV$.

Received 19 August 2022; Received in revised form 6 September 2022; Accepted 14 September 2022;
Available online 25 September 2022;
doi: 10.46291/ICONTECHvol6iss3pp12-29

Conclusions

In this study, the structural and spectroscopic properties of 4- ({4- [Bis (2-cyanoethyl) amino] phenyl} diazinyl) benzene sulfonamide ($C_{18}H_{18}N_6O_2S$) azo dye have been investigated by using DFT/B3LYP method with the basis set of 6-311G(d,p). The linear correlation between the experiment and the DFT method for the structural properties such as bond length and bond angles has been calculated. FT-IR analysis shows that title azo dye owns 129 vibrational normal modes including mainly stretching, bending, and torsion mode. The absorbance spectra have been obtained in six different solvation by using the method of TD-DFT/B3LYP. It is shown that the solvation has not a significant effect on the absorption peaks. The absorbance peaks appear at the wavelength of ~ 428 nm. Moreover, ^{1}H and ^{13}C chemical shifts concerning TMS have been identified to characterize the title compound. Finally, HOMO-LUMO energy values for the title compound reveal the electronic behavior of the title azo dye, such as high ionization potential energy, electron affinity, and electronegativity, but with low chemical hardness. In the future, it is expected that the results of this study will lead to experimental studies and will be used as supporting data.

Acknowledgement

This study has been supported by Pamukkale University (Grant No: 2021FEBE063).

References

1. Ziarani GM, Moradi R, Lashgari N, G.Kruger H. Azo Dyes. In: *Metal-Free Synthetic Organic Dyes*. ELSEVIER; 2018:47-93. doi:https://doi.org/10.1016/B978-0-12-815647-6.00004-2
2. Kunz A, Oberhof N, Scherz F, Martins L, Dreuw A, Wegner HA. Azobenzene-Substituted Triptycenes: Understanding the Exciton Coupling of Molecular Switches in Close Proximity. *Chem - A Eur J*. 2022;28(e202200972):1-6. doi:10.1002/chem.202200972
3. Ali Y, Hamid SA, Rashid U. Biomedical Applications of Aromatic Azo Compounds. *Natl Libr Med Natl Cent Biotechnol Inf*. 2018;10(3):107778.
4. Liu X, Liang M, Liu M, et al. Highly Efficient Catalysis of Azo Dyes Using Recyclable Silver Nanoparticles Immobilized on Tannic Acid-Grafted Eggshell Membrane. *springerOpen*. 2016;11(440).
5. Asifa MF, Banob R, Farooq R, et al. Shedding light on the second order nonlinear optical responses of commercially available acidic azo dyes for laser applications. *Dye Pigment ELSEVIER*. 2022;202(110284). doi:https://doi.org/10.1016/j.dyepig.2022.110284
6. Alsantali RI, Raja QA, Alzahrani AYA, et al. Miscellaneous azo dyes: a comprehensive review on recent advancements in biological and industrial applications. *Dye Pigment ELSEVIER*. 2022;199(110050). doi:https://doi.org/10.1016/j.dyepig.2021.110050
7. Huang Y, Ye Q, Li J, Zheng M, Yan B. Preparation of a redox mediator membrane and its application to catalyzing biodegradation of azo dyes. *J Environ Chem Eng ELSEVIER*. 2022;10(3):107778. doi:https://doi.org/10.1016/j.jece.2022.107778
8. Gervasio G, Marabello D, Bertolotti F. 4-({4-[Bis(2-cyanoethyl)amino]phenyl}diazenyl)benzenesulfonamide. *Acta Crystallogr Sect E*. 2010;E67(December):1600-5368. doi:10.1107/S1600536810053158
9. Lewars EG. *Computational Chemistry: Introduction to the Theory and Applications of Molecular and Quantum Mechanics*. (Lewars E, ed.).; 2011. doi:10.1007/978-90-481-3862-3
10. Åstrand PO, Bak KL, Sauer SP. Ab initio calculations on 2-imidazolyl-2-thiazolyl azo compounds

Received 19 August 2022; Received in revised form 6 September 2022; Accepted 14 September 2022;
Available online 25 September 2022;
doi: 10.46291/ICONTECHvol6iss3pp12-29

– an investigation of potential near-infrared absorbing structures. *Chem Phys Lett*. 2001;343(1-2):171-177. doi:https://doi.org/10.1016/S0009-2614(01)00673-X

11. Funar-Timofei S, Fabian WMF, Kurunczi L, Goodarzi M, Ali ST, Heydend Y Vander. Modelling heterocyclic azo dye affinities for cellulose fibres by computational approaches. *Dye Pigment ELSEVIER*. 2012;94(2):278-289. doi:https://doi.org/10.1016/j.dyepig.2012.01.015
12. Atay ÇK, Kart SÖ, Gökalp M, Tuğrul Ö, Tilki T. Characterization and absorption properties of newly synthesized mono azo dyes: Experimental and theoretical approach. *J Mol Struct*. 2019;1180:251-259. doi:https://doi.org/10.1016/j.molstruc.2018.11.108
13. Tasli PT, Atay ÇK, Demirturk T, Tilki T. Experimental and computational studies of newly synthesized azo dyes based materials. *J Mol Struct*. 2020;1201:127098. doi:https://doi.org/10.1016/j.molstruc.2019.127098
14. R M, S K. Data depth approach in fitting linear regression models. In: *Materialstoday: Proceedings*. ; 2022:2212-2215. doi:https://doi.org/10.1016/j.matpr.2021.12.321
15. Pavia DL, Lampman GM, Kriz GS, R.Vyvyan J. *Introduction to Spectroscopy*. 5th ed. Nelson Education; 2015. doi:10.1201/b21879-2
16. Trani F, Scalmani G, Zheng G, Carnimeo I, Frisch M, Barone V. Time-Depent Density Functional Tight Binding: New Formulation and Benchmark of Excited States. *J Chem Educ Comput*. 2011;7(10):3304-3313. doi:https://dx.doi.org/10.1021/ct200461y
17. Basis Sets Gaussian. Expanding the Limits of Computational Chemistry. Published 2021. https://gaussian.com/basissets/
18. Seeman JI. *Kenichi Fukui, Frontier Molecular Orbital Theory, and the Woodward-Hoffmann Rules. Part II. A Sleeping Beauty in Chemistry†***. Vol 22.; 2022. doi:10.1002/tcr.202100300
19. Axel D. Becke. Density-functional exchange-energy approximation with correct asymptotic behavior. *Phys Rev Am Phys Soc*. 1988;A38(3098). doi:https://doi.org/10.1103/PhysRevA.38.3098
20. Lee TD, Yang CN. Many-Body Problem in Quantum Mechanics and Quantum Statistical Mechanics. *Phys Rev Am Phys Soc*. 1957;105(3). doi:doi:10.1103/physrev.105.1119
21. Cincinnati. Software in Chem-Bio Library. Published 2021. https://guides.libraries.uc.edu/c.php?g=222784&p=1473460
22. Frisch MJ. Gaussian 09. Published online 2016. https://gaussian.com/g09citation/
23. Beşergil B. FTIR Absorpsiyon Spektroskopisi (FTIR absorption spectroscopy). Published 2022. http://bilsenbesergil.blogspot.com/p/8_44.html
24. Jamróz MH. Spectrochimica Acta Part A : Molecular and Biomolecular Spectroscopy Vibrational energy distribution analysis (VEDA): Scopes and limitations. *Spectrochim Acta Part A Mol Biomol Spectrosc ELSEVIER*. 2013;114:220-230. doi:10.1016/j.saa.2013.05.096
25. *Vibrational Frequency Scaling Factors*.; 2022. https://cccbdb.nist.gov/vsfx.asp
26. Tomilin F, Rogova A, Kaufman E, Drevolsky A, Gerasimova M, Slyusareva E. Solvent effect in the theoretical absorption and emission spectra of fluorescein dyes. Published online 2019:29. doi:10.1117/12.2548739
27. Naser naser A, Musa MK, Hussein AA, Saleh ZK. Solvent effects on the electronic absorption spectra of Thymol. *Chem Educ*. 2015;20:176-182. doi:10.1080/00387018808082360
28. Wolinski K, Haacke R, Hinton JF, Pulay P. Methods for parallel computation of SCF NMR chemical shifts by GIAO method: Efficient integral calculation, multi-Fock algorithm, and pseudodiagonalization. *J Comput Chem*. 1998;18(6):816-825. doi:https://doi.org/10.1002/(SICI)1096-987X(19970430)18:6<816::AID-JCC7>3.0.CO;2-V
29. Spivey AC. *Advanced Chemistry Topics 1 – Pericyclic Reactions LECTURE 4 The Frontier Molecular Orbital (FMO) Approach Format & Scope of Lecture 4*.; 2022.

Received 19 August 2022; Received in revised form 6 September 2022; Accepted 14 September 2022;
Available online 25 September 2022;
doi: 10.46291/ICONTECHvol6iss3pp12-29

https://www.imperial.ac.uk/media/imperial-college/research-centres-and-groups/spivey-group/teaching/pericyclic-reactions/2122---Lecture-4---The-FMO-Approach---All-Parts.pdf

30. Tawada Y, Tsuneda T, Yanagisawa S. A long-range-corrected time-dependent density functional theory. *J Chem Phys*. 2004;120(8425):113-8656. doi:https://doi.org/10.1063/1.1688752
31. Guido C, Capraseccar S. How to perform corrected Linear Response calculations in G09 Corrected Linear Response State-specific correction to solvent polarization response Usage in Gaussian. *Mol Pisa*. 2016;(March):1-7. doi:10.13140/RG.2.1.1903.7845
32. Metin Balci. Chemical Shift. In: *Basic 1H- and 13C-NMR Spectroscopy*. ; 2005:25-85.
33. Vaníček J, Begušić T. Ab Initio Semiclassical Evaluation of Vibrationally Resolved Electronic Spectra With Thawed Gaussians. In: *Molecular Spectroscopy and Quantum Dynamics*. ; 2021:199-229. doi:https://doi.org/10.1016/B978-0-12-817234-6.00011-8
34. Hsu SL, Patel J, Zhao W. Vibrational Spectroscopy of Polymers. In: *Molecular Characterization of Polymers A Fundamental Guide*. ; 2021:369-407. doi:https://doi.org/10.1016/B978-0-12-819768-4.00010-5
35. Lauro C di. Expansion and Transformations of the Vibration-Rotation Hamiltonian. In: *Rotational Structure in Molecular Infrared Spectra*. 2nd ed. ; 2020:97-107. doi:https://doi.org/10.1016/B978-0-12-821336-0.00006-7
36. Michał H.Jamróz, Warsaw. Vibrational Energy Distribution Analysis (VEDA). Published online 2010. https://smmg.pl/software/veda
37. Gauglitz G, Vo-Dinh T. *Handbook of Spectroscopy*. Wiley-VCH; 2002.
38. The Beer Lambert Law. EDINBURGH Instruments. Published 2022. https://www.edinst.com/us/blog/the-beer-lambert-law/
39. Beauchamp P. Infrared Tables (short summary of common absorption frequencies). *Course Notes*. 2010;2620:19.
40. Beşergil B. Nükleer Magnetik Rezonans; Tanımlar (NMR; definitions). Published 2022. http://bilsenbesergil.blogspot.com/p/blog-page_588.html
41. Singh MK, Singh A. Nuclear magnetic resonance spectroscopy. In: *Characterization of Polymers and Fibers The Textile Industrial Book Series*. WP Woodhead Publishing; 2022:321-339. doi:https://doi.org/10.1016/B978-0-12-823986-5.00011-7
42. Carreras HZ. NMR SPectroscopy Principles, Interpreting an NMR Spectrum and Common Problems. Technology Networks Analysis and Separations. Published 2021. https://www.technologynetworks.com/analysis/articles/nmr-spectroscopy-principles-interpreting-an-nmr-spectrum-and-common-problems-355891
43. Metin Balci. *Basic 1H- and 13C-NMR Spectroscopy*. 1st ed.; 2005.
44. E.Crowley T. Nuclear magnetic resonance spectroscopy. In: *Purification and Characterization of Secondary Metabolites A Laboratory Manual for Analytical and Structural Biochemistry*. Academic Press; 2020:67-78. doi:https://doi.org/10.1016/B978-0-12-813942-4.00007-3
45. Antony ID, Kores JJJ, Sasitha T, Jebaraj JW. DFT, NBO, HOMO-LUMO, NCI, stability, Fukui function and hole – Electron analyses of tolcapone. *Comput Theor Chem*. 2021;1202:113296. doi:https://doi.org/10.1016/j.comptc.2021.113296
46. Salami N, Shokri A. Electronic structure of solids and molecules. In: *Interface Science and Technology*. ; 2021:325-373. doi:https://doi.org/10.1016/B978-0-12-818806-4.00002-4
47. Pilli SR, Banerjee T, Mohanty K. HOMO–LUMO energy interactions between endocrine disrupting chemicals and ionic liquids using the density functional theory: Evaluation and comparison. *J Mol Liq ELSEVIER*. 2015;207:112-124. doi:https://doi.org/10.1016/j.molliq.2015.03.019Get
48. Musiał M, Cembrzyńska J, Meissner L. Potential Energy Curves via Double Ionization Potential

Received 19 August 2022; Received in revised form 6 September 2022; Accepted 14 September 2022; Available online 25 September 2022;
doi: 10.46291/ICONTECHvol6iss3pp12-29

Calculations: Example of HF Molecule. In: *Advance in Quantum Chemistyr*. ; 2014:153-172. doi:https://doi.org/10.1016/B978-0-12-800536-1.00008-3

49. Bassi H, Shah N, Chu S, Clark J, Clark J. Electron Affinity. Chemistry LibreText. Published 2022. https://chem.libretexts.org/Bookshelves/Physical_and_Theoretical_Chemistry_Textbook_Maps/Supplemental_Modules_(Physical_and_Theoretical_Chemistry)/Physical_Properties_of_Matter/Atomic_and_Molecular_Properties/Electron_Affinity
50. Clark J, Bank R. Electronegativity. Chemistry LibreText. Published 2021. https://chem.libretexts.org/Bookshelves/Physical_and_Theoretical_Chemistry_Textbook_Maps/Supplemental_Modules_(Physical_and_Theoretical_Chemistry)/Physical_Properties_of_Matter/Atomic_and_Molecular_Properties/Electronegativity
51. Kaya S, Kaya C. A new method for calculation of molecular hardness: A theoretical study. *Comput Theor Chem*. 2015;1060:66-70. doi:10.1016/j.comptc.2015.03.004
52. Perez P, Domingo LR, Aizman A, Contreras R. The Electrophilicity Index in Organic Chemistry. *Theor Comput Chem*. 2007;19:139-201. doi:10.1016/S1380-7323(07)80010-0

Received 19 August 2022; Received in revised form 6 September 2022; Accepted 14 September 2022; Available online 25 September 2022;
doi: 10.46291/ICONTECHvol6iss3pp12-29